RESEARCH ARTICLE

*National Science Review*
7: 21–26, 2020
doi: 10.1093/nsr/nwz129
Advance access publication 2 September 2019

PHYSICS

# Superconductivity in chromium nitrides $Pr_3Cr_{10-x}N_{11}$ with strong electron correlations

Wei Wu[1,2], Kai Liu[3], Yanjie Li[1,2], Zhenhai Yu[4], Desheng Wu[1,2], Yuting Shao[1,2], Shihang Na[1,2], Gang Li[1,5], Ruizhen Huang[2,6], Tao Xiang[1,2,6] and Jianlin Luo[1,2,5,*]

[1]Beijing National Laboratory for Condensed Matter Physics and Institute of Physics, Chinese Academy of Sciences, Beijing 100190, China; [2]School of Physical Sciences, University of Chinese Academy of Sciences, Beijing 100190, China; [3]Department of Physics and Beijing Key Laboratory of Opto-electronic Functional Materials & Micro-nano Devices, Renmin University of China, Beijing 100872, China; [4]School of Physical Science and Technology, ShanghaiTech University, Shanghai 201210, China; [5]Songshan Lake Materials Laboratory, Dongguan 523808, China and [6]Kavli Institute for Theoretical Sciences, Beijing 100190, China

*Corresponding authors. E-mail: jlluo@iphy.ac.cn

**Received** 14 June 2019; **Revised** 14 August 2019; **Accepted** 15 August 2019

## ABSTRACT

Exploration of superconductivity in Cr-based compounds has attracted considerable interest because only a few Cr-based superconductors (CrAs, $A_2Cr_3As_3$ and $ACr_3As_3$ (A = K, Rb, Cs, Na)) have been discovered so far and they show an unconventional pairing mechanism. We report the discovery of bulk superconductivity at 5.25 K in chromium nitride in $Pr_3Cr_{10-x}N_{11}$ with a cubic lattice structure. A relatively large upper critical field of $H_{c2}(0) \sim 12.6$ T is determined, which is larger than the estimated Pauli-paramagnetic pair-breaking magnetic field. The material has a large electronic specific-heat coefficient of 170 mJ $K^{-2}$ $mol^{-1}$—about 10 times larger than that estimated by the electronic structure calculation, which suggests that correlations between 3d electrons are very strong in $Pr_3Cr_{10-x}N_{11}$, and thus quantum fluctuations might be involved. Electronic structure calculations show that the density of states at the Fermi energy are contributed predominantly by Cr 3d electrons, implying that the superconductivity results mainly from the condensation of Cr 3d electrons. $Pr_3Cr_{10-x}N_{11}$ represents a rare example of possible unconventional superconductivity emerging in a 3D system with strong electron correlations. Nevertheless, clarification of the specific pairing symmetry needs more investigation.

**Keywords:** Cr-based superconductors, nitrides, strong electron correlations, unconventional superconductivity

## INTRODUCTION

The 3d transition-metal oxides or pnictides exhibit rich quantum phases with novel quantum states, such as long-range magnetic orders, charge or spin density waves, metal-insulator transitions, high-$T_c$ superconductivity and colossal magnetoresistance. In particular, unconventional high-$T_c$ superconductivity has been discovered in cuprates as well as in iron-based superconductors [1,2]. Many compounds with 3d transition-metal elements can become superconducting at low temperatures. However, it is relatively difficult to find a superconducting material in chromium-based compounds because most Cr-based compounds have strong magnetism, which generally is not in favor of superconductivity. In fact, CrAs, $A_2Cr_3As_3$ and $ACr_3As_3$ (A = Na, K, Rb, Cs) are the only Cr-based superconductors so far [3–6].

Superconductivity in CrAs was discovered in 2014 [3,4]. CrAs undergoes a first-order antiferromagnetic transition with a double helical spin structure at $T_N \approx 265$ K [3,7,8]. A bulk superconductivity with $T_c \approx 2$ K emerges above a pressure $P_c \approx 8$ kbar, where the antiferromagnetic order is completely suppressed. Both the NMR and neutron-scattering measurements for CrAs under high pressure revealed that there are strong magnetic fluctuations and line nodes may exist in the superconducting gap function [9–13], as in $Sr_2RuO_4$ or some heavy fermion superconductors [14,15]. After the discovery of superconductivity in CrAs, superconductivity has also been found in the quasi-1D compounds $A_2Cr_3As_3$ (A = K, Rb, Cs) [3,4]. The upper critical field $H_{c2}$ of $K_2Cr_3As_3$ is about three times larger than the Pauli-paramagnetic limit.

In this paper, we report a novel Cr-based nitride superconductor with a cubic structure, $Pr_3Cr_{10-x}N_{11}$, which was first synthesized and characterized by Broil *et al.* in 1995 [16]. The compound crystallizes in space group *Fm*-3*m* (No. 225)

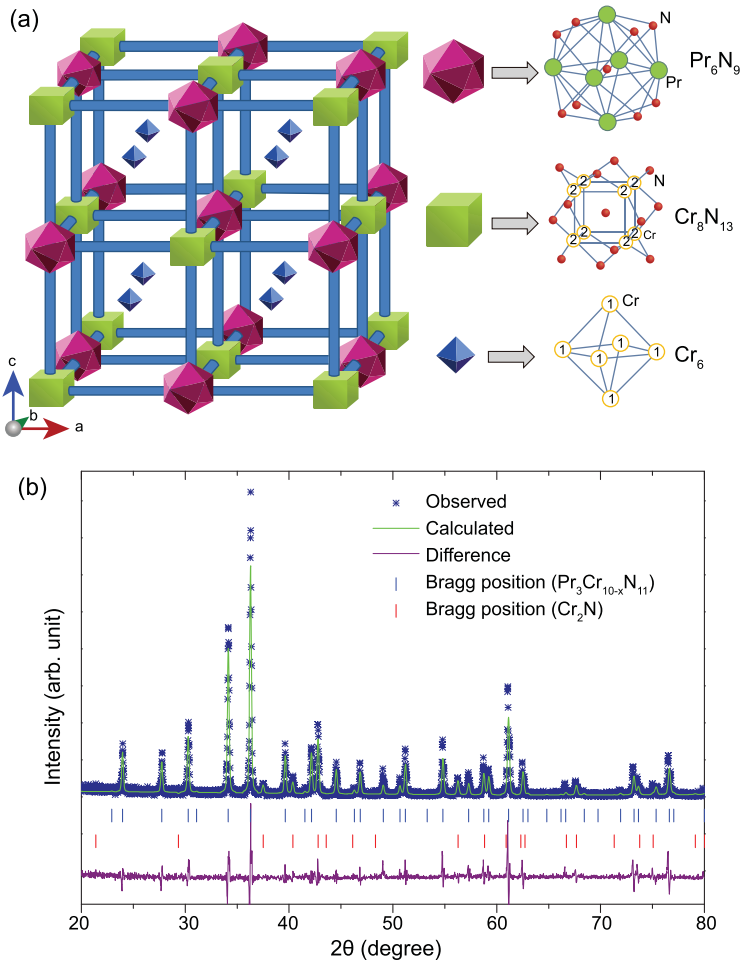


**Figure 1.** (a) The face-centered cubic cell of $Pr_3Cr_{10-x}N_{11}$ with three kinds of building blocks: $Pr_6N_9$, $Cr_8N_{13}$ and $Cr_6$, respectively. The blocks are shown in a shrunken form. There are two Cr positions: Cr1 and Cr2. (b) Typical Rietveld refinement of $Pr_3Cr_{10-x}N_{11}$ under ambient conditions. The vertical bars represent the calculated Bragg reflection positions of the diffraction peaks for $Pr_3Cr_{10-x}N_{11}$. The difference between the observed (scatters) and the fitted patterns (line) is shown at the bottom of the diffraction peaks.

with lattice constant $a = 12.891$ Å. It contains 192 atoms in a face-centered cubic (FCC) cell with three kinds of building blocks, as illustrated in Fig. 1a. The building blocks are $Pr_6N_9$, $Cr_8N_{13}$ and $Cr_6$. Previous studies showed that there are Cr vacancies in the lattice structure. However, no low-temperature physical properties were reported [16,17]. Our key finding of this study is the observation of superconductivity in $Pr_3Cr_{10-x}N_{11}$ with $T_c \sim 5.25$ K. The high-quality samples have a shielding fraction of 85% at 2 K from zero-field-cooled (ZFC) magnetic susceptibility and a prominent superconducting peak in the specific-heat measurement. A relatively large upper critical field is found at the zero-temperature limit, $H_{c2}(0) \sim 12.6$ T, which is larger than the Pauli-paramagnetic pair-breaking field. From electronic structure calculations, we find that the density of states (DOS) at the Fermi energy are predominately contributed by Cr 3d electrons. The present results demonstrate that $Pr_3Cr_{10-x}N_{11}$ is the first Cr-based superconductor discovered in chromium nitrides and it represents a rare example that possibly unconventional superconductivity emerges in a 3D system with strong electron correlations.

## RESULTS AND DISCUSSION

### Sample and characterization

Polycrystalline samples of $Pr_3Cr_{10-x}N_{11}$ were prepared by direct reactions of the corresponding binary nitrides with solid reaction. Synthesized powder shows a dark-brown color and is air-sensitive, as it is easily oxidized to $Pr_2O_3$ within a few hours. Figure 1b shows the General Structure Analysis System (GSAS) refinement of $Pr_3Cr_{10-x}N_{11}$ under ambient conditions, which indicates that $Pr_3Cr_{10-x}N_{11}$ crystallized in an FCC structure with space group *Fm*-3*m*. All the $Pr_3Cr_{10-x}N_{11}$ reflections can be well indexed based on a cubic cell with lattice parameter $a = 12.8521$ Å, which is consistent with those reported in the literature ($a = 12.891$ Å) [16], indicating their ideal composition. A small amount of raw reactant $Cr_2N$ was marked with a red vertical bar.

### Temperature-dependent resistivity in $Pr_3Cr_{10-x}N_{11}$

Figure 2a shows the temperature-dependent resistivity for $Pr_3Cr_{10-x}N_{11}$ from 1.8 to 300 K at zero field. The normal-state resistivity is metallic, with no phase transition observed. At low temperatures, a sharp superconducting transition is observed with onset $T_c$ of about 5.25 K, as shown in the inset of Fig. 2a. The $T_c$ of $Pr_3Cr_{10-x}N_{11}$ is higher than that of CrAs with $T_{max} \sim 2$ K under pressure and is close to $K_2Cr_3As_3$ with $T_c \sim 6.1$ K [12].

The new superconductor $Pr_3Cr_{10-x}N_{11}$ shows a relatively large upper critical field. Figure 2b shows resistivity data in magnetic fields up to 9 T. As the field increases, the transition temperature $T_c$ shifts to a lower temperature and the transition width is gradually broadened, similar to the iron-based superconductors [18,19]. The upper critical field $H_{c2}$ (T) curve obtained from the field-dependent transition temperatures shows a remarkably high critical field of 12.6 T using the formula $H_{c2}(T) = H_{c2}(0)(1 - t^2)$, where $t$ is the reduced temperature $t = T/T_c$ and of 22 T using the Werthamer–Helfand–Hohenberg (WHH) theory [20]. On the other hand, the Pauli-paramagnetic limit for the upper critical field is $H_P = 1.84T_c \approx 9.6$ T in the case of an isotropic full

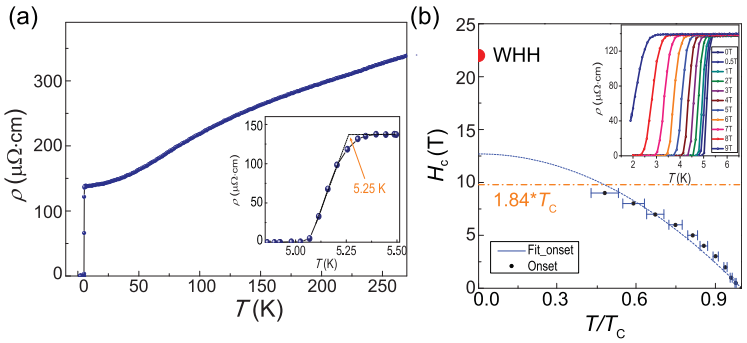


**Figure 2.** (a) Temperature dependence of the resistivity for $Pr_3Cr_{10-x}N_{11}$ from 1.8 to 300 K at the zero field. The inset shows the resistivity near superconducting transition. (b) The temperature dependence of the upper critical magnetic field. The solid circle shows the upper critical field obtained from WHH fitting. The inset shows the temperature dependence of the resistivity at different fields.

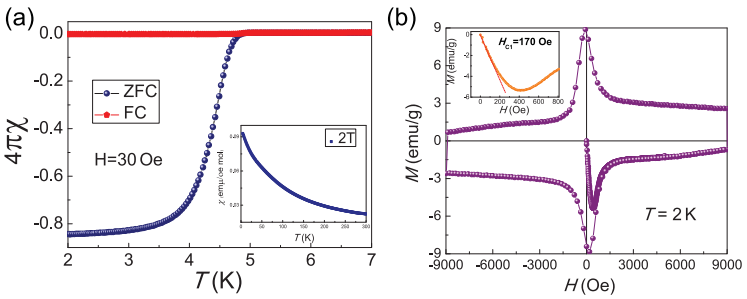


**Figure 3.** (a) Temperature dependence of the dc magnetic susceptibility with zero field cool (ZFC) and field cool (FC) measured in a field of 30 Oe. The inset of Fig. 3a is the normal-state susceptibility measured in a field of 2 T. (b) The magnetic hysteresis of the sample measured at 2 K. The left inset shows the lower critical magnetic field.

superconducting gap without considering spin–orbit coupling [21,22]. The $H_{c2}$ (0) in $Pr_3Cr_{10-x}N_{11}$ is 130% as large as $H_P$. Usually, the high superconducting upper critical field can be originated from multi-band effects, the strong-coupling effect, the spin-triplet pairing and the strong spin–orbit coupling effect in a low-dimensional system [23–25]. The origin of large $H_{c2}(0)$ in $Pr_3Cr_{10-x}N_{11}$ needs to be further studied. The obtained $\mu_0 H_{c2}(0)$ allows us to estimate the Ginzburg–Landau coherence length $\xi =$ 51 Å according to the relationship: $\mu_0 H_{c2}(0) = \Phi_0/2\pi\xi^2$, where $\Phi_0 = 2.067 \times 10^{-15}$ Wb is the magnetic flux quantum.

## Magnetic-susceptibility measurements in $Pr_3Cr_{10-x}N_{11}$

The bulk superconductivity in $Pr_3Cr_{10-x}N_{11}$ was confirmed by magnetic-susceptibility measurements. Figure 3a shows susceptibility $\chi$ at low temperatures with ZFC and field cool (FC) under a magnetic field of 30 Oe. $\chi$ starts to drop below $T_c$ and the diamagnetic signal tends to saturate at low temperatures. The shielding fraction estimated from the ZFC magnetic susceptibility at 2 K is 85%, confirming bulk superconductivity in the sample. The normal-state susceptibility $\chi$ increases with decreasing temperature in $Pr_3Cr_{10-x}N_{11}$, showing a Curie–Weiss behavior as shown in the inset of Fig. 3a. Such behavior is different from that of isostructural material $La_3Cr_{10-x}N_{11}$, which shows a Pauli paramagnetism with a nearly temperature-independent susceptibility [16]. Since $La^{3+}$ ion has no occupied 4f electrons while each $Pr^{3+}$ ion has two occupied 4f electrons, it is natural to attribute the Curie–Weiss behavior of $\chi$(T) in $Pr_3Cr_{10-x}N_{11}$ to the magnetic moments of $Pr^{3+}$ 4f electrons. Using a Curie–Weiss fit with formula $\chi(T) = \chi_0 + C/(T-\theta)$, we obtained the effective moment of each Pr ion at about 3.6 $\mu_B$, which is very close to the calculated moment of 3.5 $\mu_B$ for $Pr^{3+}$ by Hund's rule. The negative value of $\theta$ indicates the correlations between Pr ions are antiferromagnetic.

Further confirmation of superconductivity is shown by the magnetic hysteresis of the sample measured at 2 K in Fig. 3b, which displays the typical magnetic hysteresis curve for a type-II superconductor. From the inset of Fig. 3b, the lower critical magnetic fields $H_{c1}$ of 170 Oe can be obtained.

## Specific-heat measurements

Figure 4a shows the specific-heat coefficient $C/T$ as a function of $T^2$ from 2 to 10 K at the zero field. The bulk nature of superconductivity is confirmed by a pronounced anomaly around $T_c = 5.25$ K, consistently with the resistivity and susceptibility measurements. Extrapolating $C/T$ to zero temperature gives a residual value of $\gamma_0 = 0.061$ mJ $g^{-1}$ $K^{-2}$. As indicated previously, there is raw reactant phase $Cr_2N$ in the sample. We measured the specific heat of $Cr_2N$ and found that it can be well fitted by $C = \gamma T + \beta T^3$ below 10 K with $\gamma = 22$ mJ $mol^{-1}$ $K^2$ and $\beta =$ 0.0373 mJ $mol^{-1}$ $K^4$. Given the residual specific-heat $\gamma_0$ origin from the $Cr_2N$ phase, we can then obtain the specific heat of pure $Pr_3Cr_{10-x}N_{11}$ by subtracting that of $Cr_2N$ from the total specific heat, as shown in the inset of Fig. 4a.

Above $T_c$, the good linear $T^2$ dependence of $C/T$ indicates that the normal-state specific heat consists of two parts of contributions: the electronic part, which is proportional to $T$, and the phonon part, which is proportional to $T^3$ at low temperatures. By fitting the normal-state specific heat C with the formula $C = \gamma_n T + \beta T^3$, we find that $\gamma_n =$ 173 mJ $K^{-2}$ $mol^{-1}$ and $\beta = 1.186$ mJ $K^{-4}$ $mol^{-1}$. The normal-state electronic coefficient $\gamma_n$ is proportional to the DOS at the Fermi level. Assuming that most of the DOS comes from the Cr 3d electrons, the value of $\gamma_n$ per mole Cr is $\gamma_n =$

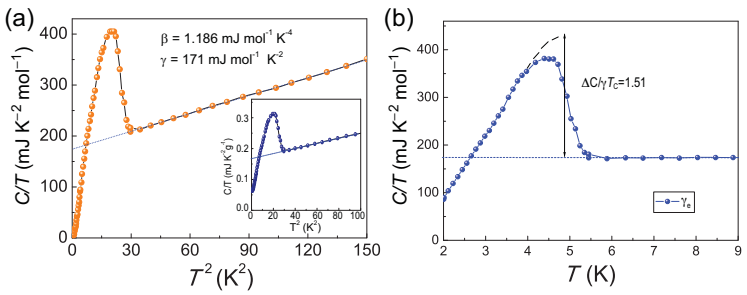


**Figure 4.** (a) The specific-heat coefficient $C/T$ of $Pr_3Cr_{10-x}N_{11}$ as a function of $T^2$. The inset shows $C/T$ versus $T^2$ for a sample with $Cr_2N$. (b) Temperature dependence of normalized electronic specific-heat $C_e/T$.

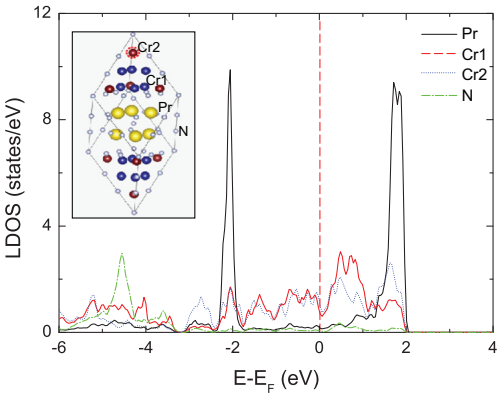


**Figure 5.** Local density of states (LDOS) for Pr, Cr1, Cr2 and N atoms in $Pr_3Cr_{9.5}N_{11}$. Inset shows a primitive cell with the yellow, blue, maroon and gray balls representing Pr, Cr1, Cr2 and N atoms, respectively. The atomic vacancy at the Cr2 site is highlighted by a red dashed circle.

17.3 mJ $K^{-2}$ mol $Cr^{-1}$ for $Pr_3Cr_{10-x}N_{11}$, which is much larger than the corresponding value for CrAs (~7 mJ $K^{-2}$ $mol^{-1}$) and MnP (~8.3 mJ $K^{-2}$ $mol^{-1}$) at ambient pressure [11,26] and it is slightly less than that for $K_2Cr_3As_3$ (~23.3 mJ $K^{-2}$ mol $Cr^{-1}$) and $KCr_3As_3$ (~27.1 mJ $K^{-2}$ mol $Cr^{-1}$) [14,27,28]. The relatively large $\gamma_n$ for $Pr_3Cr_{10-x}N_{11}$ indicates strong correlations of Cr 3d electrons. The Debye temperature $\theta_D$ obtained from $\beta$ is 339 K.

In Fig. 4b, the normalized specific-heat jump at $T_c$ is found to be $\Delta C/\gamma_n T_c = 1.51$. This value is much smaller than those of $K_2Cr_3As_3$ (~2.5) and LaNiAsO (~1.9), which are regarded as strong-coupling superconductivity [14,27,29]. The normalized $\Delta C/\gamma_n T_c$ reflects the coupling strength between the conducting electrons and the pairing glue. We can then estimate the electron–phonon coupling constant $\lambda = 0.6$ from the modified McMillian formula [25,30,31]:

$$\lambda = \frac{1.04 + \mu^* \ln(\omega/1.2T_c)}{(1 - 0.62\mu^*)\ln(\omega/1.2T_c) - 1.04}$$

where $\mu^*$ is a Coulomb pseudopotential and $\omega$ is a logarithmic averaged phonon frequency. $\omega$ can be determined from the specific-heat jump at $T_c$ using the formula: $\Delta C/\gamma_n T_c = 1.43[1 + 53(T_c/\omega)2\ln(\omega/3T_c)]$. Taking $\mu^* = 0.10$ and $T_c = 5.25$ K, we obtained $\omega = 320$ K and $\lambda = 0.6$. For such a small electron–phonon coupling constant, the large $H_{c2}(0)$ value is not likely due to the strong-coupling effect.

## Theoretical calculations

In order to examine which atomic species contribute most around the Fermi level ($E_F$), we have plotted the local density of states (LDOS) for $Pr_3Cr_{9.5}N_{11}$ as shown in Fig. 5. Electronic structure calculations show that the DOS at the Fermi energy are contributed predominantly by Cr 3d electrons, implying that the superconductivity results mainly from the condensation of Cr 3d electrons similar to that in CrAs [32]. The primitive cell of $Pr_3Cr_{10-x}N_{11}$ is shown in the inset of Fig. 5, in which there are two types of nonequivalent Cr atoms, labeled as Cr1 and Cr2, respectively. Both the Cr1 and Cr2 atoms have large contributions around $E_F$, mainly originating from the 3*d* orbitals of Cr atoms. In contrast, the vast majority of states for Pr and N atoms are far from the Fermi level. A higher density of Cr2 vacancies, such as in $Pr_3Cr_9N_{11}$, does not change the results very much. According to our calculations, the total DOS of $Pr_3Cr_{9.5}N_{11}$ at the Fermi level $N(E_F)$ is 7.37 states/(eV∗f.u.). As a result, the corresponding calculated electronic specific-heat coefficient $\gamma_e$ is 17.4 mJ $K^{-2}$ $mol^{-1}$. Experimentally, the measured $\gamma_e$ for $Pr_3Cr_{10-x}N_{11}$ is about 173 mJ $K^{-2}$ $mol^{-1}$—about 10 times more than the band calculations, which indicates the strong mass-enhancement effect.

## CONCLUSION

Superconductivity in $Pr_3Cr_{10-x}N_{11}$ shows several novel characters. First, electronic structure calculations show that most of DOS at Fermi energy is contributed by Cr 3*d* electrons, suggesting that the superconductivity is originated from the condensation of Cr 3*d* electrons. So $Pr_3Cr_{10-x}N_{11}$ is the first Cr-based superconductor discovered in nitrides. A few other known Cr-based superconductors (CrAs, $A_2Cr_3As_3$ and $ACr_3As_3$ (A = K, Rb, Cs, Na)) are arsenide. Superconductivity in CrAs emerges in the vicinity of a quantum critical point and antiferromagnetic spin fluctuations associated with the quantum criticality could act as an important glue medium for Cooper pairing. Superconductivity in the quasi-1D compounds $A_2Cr_3As_3$

(A = K, Rb, Cs) shows non-s-wave pairing. Both of them show an unconventional pairing mechanism. So the Cr d-electrons play an important role in electron correlations and possibly unconventional superconductivity in $Pr_3Cr_{10-x}N_{11}$ with Cr d-electrons.

Second, $Pr_3Cr_{10-x}N_{11}$ has a relatively large upper critical field $H_{c2}(0) \sim 12.6$ T, exceeding the Pauli limit of the paramagnetic pair-breaking field; this is rare in 3D-structure superconductors. The upper critical field provides very important information on the superconducting pairing. This behavior resembles that unconventional superconducting in $K_2Cr_3As_3$ in which $H_{c2}$ is three times the Pauli-paramagnetic limit that is regarded as evidence of spin-triplet superconductivity.

Last but not least, the measured $\gamma_e$ for $Pr_3Cr_{10-x}N_{11}$ is about 173 mJ $mol^{-1}$ $K^{-2}$, equivalent to 17.3 mJ $K^{-2}$ mol $Cr^{-1}$. This $\gamma$ value is close to that of $K_2Cr_3As_3$ (mJ $K^{-2}$ mol $Cr^{-1}$), indicating enhanced electron correlations in $Pr_3Cr_{10-x}N_{11}$. The experimental value of $\gamma_e$ is about 10 times higher than the electronic calculations. This large renormalization factor cannot be explained by electron–phonon interactions and thus quantum fluctuations might be involved.

In conclusion, we report the experimental result for a novel Cr-based superconductor nitrides $Pr_3Cr_{10-x}N_{11}$ with a cubic lattice structure. Bulk superconductivity with $T_c \sim 5.25$ K is observed from the resistivity, susceptibility and specific-heat measurements. Further theoretical and experimental studies are needed to determine the pairing symmetry and the corresponding mechanism, especially the role of Cr 3d electrons, for the observed superconductivity in $Pr_3Cr_{10-x}N_{11}$.

## METHODS

### Sample preparation

Polycrystalline samples of $Pr_3Cr_{10-x}N_{11}$ were prepared by direct reactions of the corresponding binary nitrides, staring with PrN (99%) and a mixture of the chromium nitrides (CrN and $Cr_2N$) in a mass ratio of 4:6. The operations were all performed in an Ar-filled glovebox. Cold-pressed pellets of the mixtures were sealed in an evacuated quartz tube ($<10^{-4}$ Pa). The pellets were gradually heated in 1 day to 1000°C, held at that temperature for 50 hours, then cooled to the room temperature in the furnace. The products were again ground in a glovebox, pressed into pellets, wrapped in Ta foil and heated in an evacuated quartz tube at 1165°C for 120 hours. It is worth noting that, after this treatment, the samples were usually still contaminated by the binary nitrides. The treatment of these samples with diluted hydrochloric acid only dissolved the rare-earth nitrides. In between these treatments, the pellets were ground to a fine powder, the decomposed rare-earth nitride was dissolved in hydrochloric acid and fresh rare -earth nitride was added again to the mixture to maintain the proper composition. The reaction temperature was carefully selected to avoid decomposition of the products, meanwhile obtaining a good crystallization. In our study, we found that $Pr_3Cr_{10-x}N_{11}$ partially decomposed above 1200°C. Synthesized powder shows a dark-brown color and is air-sensitive, as it is easily oxidized to $Pr_2O_3$ within a few hours.

### Measurements

The electrical transport measurement was carried out on a physical-property measurement system (PPMS-9, Quantum Design). The resistivity was measured by a standard four-probe method, employing silver-paste contacts cured at room temperature, used for resistivity measurements, with the electric current applied in an arbitrary direction. The magnetic susceptibility was measured in a Quantum Design SQUID VSM. The specific-heat measurements were performed up to 9 T in a PPMS.

### Theoretical modeling

We carried out first-principles electronic structure calculations on $Pr_3Cr_{10-x}N_{11}$. The first-principles calculations were performed using the projector augmented-wave method [33], as implemented in the VASP package [34]. The generalized gradient approximation of the Perdew–Burke–Ernzerhof type [35] was adopted for the exchange-correlation function.

## SUPPLEMENTARY DATA

Supplementary data are available at *NSR* online.

## ACKNOWLEDGEMENTS

The authors are grateful to Dr. Zhao Yu Liu and Prof. Shi Liang Li (Institute of Physics) for their help in experiments.

## FUNDING

This work was supported by the National Basic Research Program of China (2017YFA0302901, 2014CB921500), the National Natural Science Foundation of China (11674375, 11634015) and the Strategic Priority Research Program and Key Research Program of Frontier Sciences of the Chinese Academy of Sciences (XDB07020200).

***Conflict of interest statement.*** None declared.

## REFERENCES


1. Bednorz JG and Müller KZ. Possible high $T_c$ superconductivity in the Ba—La—Cu—O system. *Z Phys B-Condens Mat* 1986; **64**: 189–93.
2. Kamihara Y, Watanabe T and Hirano M *et al.* Iron-based layered superconductor La $[O_{1-x}F_x]$ FeAs (x = 0.05—0.12) with $T_c$ = 26 K. *J Am Chem Soc* 2008; **130**: 3296–7.
3. Wu W, Cheng JG and Matsubayashi K *et al.* Superconductivity in the vicinity of antiferromagnetic order in CrAs. *Nat Commun* 2014; **5**: 5508.
4. Kotegawa H, Nakahara S and Tou H *et al.* Superconductivity of 2.2 K under pressure in Helimagnet CrAs. *J Physical Soc Japan* 2014; **83**: 238–41.
5. Bao JK, Liu JY and Ma CW *et al.* Superconductivity in quasi-one-dimensional $K_2Cr_3As_3$ with significant electron correlations. *Phys Rev X* 2015; **5**: 5568–77.
6. Tang ZT, Bao JK and Liu Y *et al.* Unconventional superconductivity in quasi-one-dimensional $Rb_2Cr_3As_3$. *Phys Rev B* 2015; **91**: 020506; Tang ZT, Bao JK and Wang Z *et al.* Superconductivity in quasi-one-dimensional $Cs_2Cr_3As_3$ with large interchain distance. *Sci China Mater* 2015; **58**: 16–20; Mu QG, Ruan BB and Pan BJ *et al.* Superconductivity at 5 K in quasi-one-dimensional Cr-based $KCr_3As_3$ single crystals. *Phys Rev B* 2017; **96**: 140504; Liu T, Mu QG and Pan BJ *et al.* Superconductivity at 7.3 K in 133-type Cr-based $RbCr_3As_3$ single crystals. *Europhys Lett* 2017; **120**: 27006.
7. Cheng JG, Matsubayashi K and Wu W *et al.* Pressure induced superconductivity on the border of magnetic order in MnP. *Phys Rev Lett* 2015; **114**: 117001.
8. Cheng JG and Luo JL. Special issue on pressure-induced superconductivity in CrAs and MnP. *J Phys Condens Matter* 2017; **29**: 440301.
9. Kotegawa H, Nakahara S and Akamatsu R *et al.* Detection of an unconventional superconducting phase in the vicinity of the strong first-order magnetic transition in CrAs using $^{75}$As-nuclear Quadrupole resonance. *Phys Rev Lett* 2015; **114**: 117002.
10. Keller L, White JS and Frontzek M *et al.* Pressure dependence of the magnetic order in CrAs: a neutron diffraction investigation. *Phys Rev B* 2015; **91**: 020409.
11. Shen Y, Wang Q and Hao YQ *et al.* Structural and magnetic phase diagram of CrAs and its relationship with pressure-induced superconductivity. *Phys Rev B* 2016; **93**: 060503.
12. Matsuda M, Ye F and Dissanayake SE *et al.* Pressure dependence of the magnetic ground states in MnP. *Phys Rev B* 2016; **93**: 100405.
13. Matsuda M, Lin FK and Yu R *et al.* Evolution of magnetic double helix and quantum criticality near a dome of superconductivity in CrAs. *Phys Rev X* 2018; **8**: 031017.
14. Mackenzie AP, Haselwimmer RKW and Tyler AW *et al.* Extremely strong dependence of superconductivity on disorder in $Sr_2RuO_4$. *Phys Rev Lett* 1998; **80**: 161–4.
15. Mathur ND, Grosche FM and Julian SR *et al.* Magnetically mediated superconductivity in heavy fermion compounds. *Nature* 1998; **394**: 39–43.
16. Broil S and Jeitschko W. The ternary rare earth chromium nitrides $Ce_2CrN_3$ and $Ln_3Cr_{10-X}N_{11}$ with Ln = La, Ce, Pr. *Z Naturforsch B* 1995; **50b**: 905–12.
17. Chevire F, Ranjan C and Disalvo F. Synthesis, crystal and electronic structures of $La_3Cr_2N_6$. *Solid State Commun* 2009; **149**: 273–6.
18. Chen GF, Li Z and Li G *et al.* Superconducting properties of the Fe-based layered superconductor $LaFeAsO_{0.9}F_{0.1-\delta}$. *Phys Rev Lett* 2008; **101**: 057007.
19. Chen GF, Li Z and Wu D *et al.* Superconductivity at 41 K and its competition with spin-density-wave instability in layered $CeO_{1-x}F_xFeAs$. *Phys Rev Lett* 2008; **100**: 247002.
20. Werthamer NR and Helfand E. Temperature and purity dependence of the superconducting critical field, $H_{c2}$. *Phys Rev Lett* 1964; **13**: 686–8.
21. Clogston AM. Upper limit for the critical field in hard superconductors. *Phys Rev Lett* 1962; **9**: 266–7.
22. Chandrasekhar BS. A note on the maximum critical field of high-field superconductors. *Appl Phys Lett* 1962; **1**: 7–8.
23. Gurevich A. Enhancement of the upper critical field by nonmagnetic impurities in dirty two-gap superconductors. *Phys Rev B* 2003; **67**: 184515.
24. Carbotte JP. Properties of boson-exchange superconductors. *Rev Mod Phys* 1990; **62**: 1027–158.
25. Lee IJ, Chaikin PM and Naughton MJ. Exceeding the Pauli paramagnetic limit in the critical field of $(TMTSF)_2PF_6$. *Phys Rev B* 2000; **62**: 14669–72.
26. Zheng P, Xu YJ and Wu W *et al.* Orbital-dependent charge dynamics in MnP revealed by optical study. *Sci Rep* 2017; **7**: 14178.
27. Shao YT, Wu XX and Wang L *et al.* Evidence of line nodes in superconducting gap function in $K_2Cr_3As_3$ from specific-heat measurements. *Europhys Lett* 2018; **123**: 57001.
28. Mu QG, Ruan BB and Pan BJ *et al.* Dynamic instabilities in strongly correlated $VSe_2$ monolayers and bilayers. *Phys Rev B* 2017; **96**: 140524.
29. Li Z, Chen GF and Dong J *et al.* Strong-coupling superconductivity in the nickel-based oxypnictide $LaNiAsO_{1-x}F_x$. *Phys Rev B* 2008; **78**: 060504.
30. Allen PB and Dynes RC. Transition temperature of strong-coupled superconductors reanalyzed. *Phys Rev B* 1975; **12**: 905–22.
31. Klimczuk T, Ronning F and Sidorov V *et al.* Physical properties of the noncentrosymmetric superconductor $Mg_{10}Ir_{19}B_{16}$. *Phys Rev Lett* 2007; **99**: 257004.
32. Autieri C and Noce C. First principles study of structural, magnetic and electronic properties of CrAs. *Philos Mag* 2017; **97**: 3276–95.
33. Blöchl PE. Projector augmented-wave method. *Phys Rev B* 1994; **50**: 17953–79; Kresse G and Joubert D. From ultrasoft pseudopotentials to the projector augmented-wave method. *Phys Rev B* 1999; **59**: 1758–75.
34. Kresse G and Hafner J. *Ab initio* molecular dynamics for liquid metals. *Phys Rev B* 1993; **47**: 558–61; Kresse G and Furthmüller J. Efficiency of *ab-initio* total energy calculations for metals and semiconductors using a plane-wave basis set. *Comp Mater Sci* 1996; **6**: 15–50; Kresse G and Furthmüller J. Efficient iterative schemes for *ab initio* total-energy calculations using a plane-wave basis set. *Phys Rev B* 1996; **54**: 11169–86.
35. Perdew JP, Burke K and Ernzerhof M. Generalized gradient approximation made simple. *Phys Rev Lett* 1996; **77**: 3865–8.